Physica B 406 (2011) 3279–3284

Contents lists available at ScienceDirect

Physica B

journal homepage: www.elsevier.com/locate/physb

Complex impedance spectroscopic studies of $Ba(Pr_{1/2}Ta_{1/2})O_3$ ceramic

Amodini Mishra [a], S.N. Choudhary [a], K. Prasad [a,*], R.N.P. Choudhary [b]

[a] University Department of Physics, T.M. Bhagalpur University, Bhagalpur 812007, India
[b] Department of Physics and Meteorology, Indian Institute of Technology, Kharagpur 712302, India

ARTICLE INFO

Article history:
Received 9 December 2010
Received in revised form
17 May 2011
Accepted 19 May 2011
Available online 24 May 2011

Keywords:
$Ba(Pr_{1/2}Ta_{1/2})O_3$
Complex impedance
Electric modulus
Perovskites
Ac conductivity

ABSTRACT

The polycrystalline sample of $Ba(Pr_{1/2}Ta_{1/2})O_3$ was prepared by a high-temperature solid-state reaction technique. The crystal symmetry, space group and unit cell dimensions were derived from the experimental results using FullProf software. XRD analysis of the compound indicated the formation of a single-phase tetragonal structure with the space group P4/mmm (1 2 3). Impedance and electric modulus analysis were used as tools to analyze the electrical behavior of the sample as a function of frequency at different temperatures. The impedance analysis of the compound indicated a typical negative temperature coefficient of resistance behavior, and dielectric relaxation was found to be of non-Debye type. The frequency dependent maximum of the imaginary part of the electric modulus follows the Arrhenius law with activation energy of 0.15 eV. The ac conductivity data obeys double power law.

1. Introduction

Ferroelectric compounds with the perovskite structure having a general formula ABO_3 have extensively been studied because of their promising electrical characteristics and some potential applications such as multilayer capacitors, non-volatile memory devices, optoelectronic devices, etc. [1–3]. Substitution of proper cations at A and/or B sites have led to the enhancement of various physical properties suitable for device applications. Investigation of the electrical properties of these materials is desirable to predict their suitability for electronic applications. It has been observed that different relaxation processes are present in complex perovskite ceramics, which may be due to a variety of defects appearing in them during their fabrication. This brings a departure of the dielectric response from the ideal Debye behavior of the sample. A method of assessment of the relaxation behavior is through impedance and electric modulus studies. Electric modulus analyses have yielded the information about conductivity and its associated relaxation in some complex perovskites having general formula [4–10]. Most of these materials were lead based and were suitable for their use due to their high dielectric permittivity, relatively low sintering temperature and temperature dependent diffuse dielectric maxima. But the presence of lead makes these materials toxic and thus has ecological restriction. Hence there is a great demand for new environmental friendly materials. Several studies have recently been made to obtain lead-free [11–17] and low lead content electroceramics [18,19] in recent past.

Complex impedance spectroscopy is a promising nondestructive testing method for analyzing the electrical processes occurring in a compound on the application of small ac signal as input perturbation. The output response of a polycrystalline compound when plotted in a complex plane plot represents grain, grain boundary and interface properties with different time constants leading to three successive semicircles. The charge transport can be due to the charge displacement, dipole reorientation and space charge formation. These charge transport processes cause a number of different polarization mechanisms, which results in frequency dispersion or dielectric relaxation in the materials under an ac field. The frequency dependence of electrical data is interrelated to each other as: complex impedance ($Z^*(\omega)=Z'-jZ''=R_s-j/\omega C_s$), complex admittance ($Y^*(\omega)=Y'+jY''=1/R_p+j\omega C_p$), complex permittivity ($\varepsilon^*(\omega)=\varepsilon'-j\varepsilon''$) and complex modulus ($M^*(\omega)=M'+jM''$). These formalisms are interrelated as $M^*=1/\varepsilon^*=j\omega C_o Z^*=j\omega C_o(1/Y^*)$ and the loss tangent, $\tan\delta=\varepsilon''/\varepsilon'=Z'/Z''$, where R_s, C_s are the series resistance and capacitance; R_p, C_p are the parallel resistance and capacitance, respectively. Accordingly, present work reports (X-ray and its Rietveld analysis) the microstructural (SEM and EDAX) and electrical (using complex impedance spectroscopic technique) behavior of $Ba(Pr_{1/2}Ta_{1/2})O_3$ (abbreviated hereafter BPT) ceramic.

2. Experimental

A high-temperature solid-state reaction technique was used for the preparation of polycrystalline $Ba(Pr_{1/2}Ta_{1/2})O_3$ sample using the following thermochemical equation:

$$BaCO_3 + 0.25Pr_2O_3 + 0.25Ta_2O_5 \xrightarrow{\Delta} Ba(Pr_{1/2}Ta_{1/2})O_3 + CO_2(g)\uparrow$$

* Corresponding author. Tel./fax: +91 641 2501699.
E-mail address: k.prasad65@gmail.com (K. Prasad).

0921-4526/$ - see front matter © 2011 Elsevier B.V. All rights reserved.
doi:10.1016/j.physb.2011.05.040

The AR-grade chemicals ($BaCO_3$, Pr_2O_3 and Ta_2O_5) were used in stoichiometric proportion and mixed thoroughly in agate mortar for 10 h and the mixture was heated at 1350 °C for 5 h in air. The calcined powder was grounded and pelletized in the form of cylindrical disk (1.12 mm diameter and 1.02 mm thickness). The optimized sintering conditions were 1400 °C for 6 h. The completion of the reaction and the formation of the desired compound were checked by X-ray diffraction (XRD) technique. The XRD data were recorded on sintered pellet of BPT with a X-ray diffractometer (Rikagu Miniflex, Japan) at room temperature, using CuK_α radiation ($\lambda=1.5405$ Å), between 15° and 90° with a scanning speed of 5.08° min^{-1}. The *XY* (2θ vs. intensity) data obtained from this experiment were plotted with the WinPLOTR program and the angular positions of the peaks were obtained with the same program [20]. The dimensions of the unit cell, the hkl values and the space group of BPT was obtained using the TREOR program in the FullProf 2000 software package and then refinement was carried out through the profile matching routine of FullProf [21]. The Bragg peaks were modeled with pseudo-Voigt function and the background was estimated by linear interpolation between selected background points. The microstructure of the sintered BPT sample was carried out using a computer-controlled high-resolution scanning electron microscope (FEI 200 FEG Quanta).

The electrical measurements were carried out on a symmetrical cell of type Ag|BPT|Ag, where Ag is a conductive paint coated on either side of the pellet. Electrical impedance (Z), phase angle (θ), loss tangent ($\tan\delta$) and capacitance (C_p) were measured as a function of frequency 0.1 kHz to 1 MHz at different temperatures (50–450 °C) using a computer-controlled LCR Hi-TESTER (HIOKI 3532-50,Japan) interfaced with a microprocessor-controlled temperature controller (DPI–1100, Sartech International, India). The ac conductivity was calculated using the relation: $\sigma_{ac}=2\pi f\varepsilon\varepsilon_o\tan\delta$, where f, ε and $\tan\delta$ are operating frequency, dielectric constant and loss tangent, respectively.

3. Results and discussion

3.1. Structural and microstructural analysis

Rietveld refinements on the XRD data of BPT were done by selecting the space group P4/mmm (1 2 3). Fig. 1 illustrates the observed, calculated and difference XRD profiles for BPT after final cycle of refinement. It can be seen that the profiles for observed and calculated ones are perfectly matching, which are well supported by the value of $\chi^2(=2.28)$. The profile fitting procedure adopted was minimizing the χ^2 function [22]. The XRD analyses indicated that BPT has a tetragonal unit cell. The crystal data and refinement factors of BPT obtained from XRD data are depicted in Table 1.

Fig. 2 shows the EDAX pattern SEM micrograph (inset) of BPT. The peaks in the pattern were perfectly assigned to the elements present in $Ba(Pr_{1/2}Ta_{1/2})O_3$. This clearly indicated the purity of chemical composition of BPT. Irregular shaped grains of unequal sizes (~1–4 μm) distributed throughout the sample are clearly visible in the SEM-micrograph. Besides some agglomerations an abnormal grain growth was also observed in the micrograph.

3.2. Complex impedance analysis

Fig. 3 shows the variation of real part of impedance (Z') with frequency at different temperatures. It is observed that the magnitude of Z' decreases with an increase in both frequency as well as temperature, which indicates an increase in ac conductivity with rise in temperature as well as frequency. Also the Z' values for all the temperatures merge above 50 kHz, which may be due to the release of space charges as a result of reduction in the barrier properties of material with the rise in temperature and may be a responsible factor for the enhancement of ac conductivity of material with temperature at higher frequencies. Further, at low frequencies the Z' values decrease with increase in temperature, which shows negative temperature coefficient of resistance (NTCR) type behavior like that of semiconductors.

Fig. 4 shows the variation of the imaginary part of impedance (Z'') with frequency at different temperatures. The plots show that the Z'' values reach a maximum (Z''_{max}) for all temperatures and the value of Z''_{max} shifts to higher frequencies with increase in

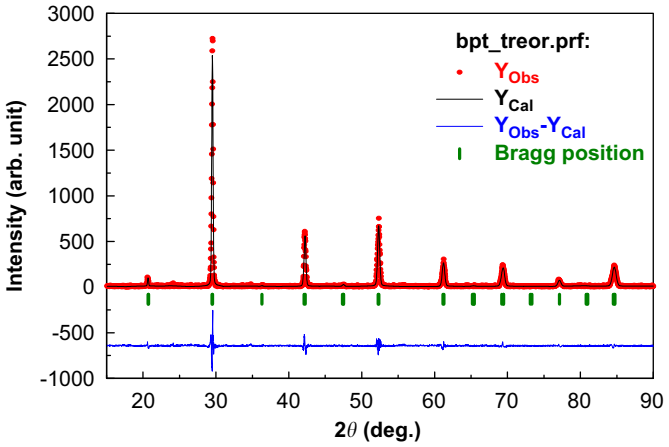

Fig. 1. Rietveld refined pattern of $Ba(Pr_{1/2}Ta_{1/2})O_3$ in the space group P4/mmm. Symbols represent the observed data points and the solid lines their Rietveld fit.

Table 1
Crystal data and refinement factors of $Ba(Pr_{1/2}Ta_{1/2})O_3$ obtained from X-ray powder diffraction data.

Parameters	Results	Description of parameters
Crystal system space group	Tetragonal P4/mmm (1 2 3)	
a (Å)	4.2758	
c (Å)	4.2908	
V (Å^3)	78.4461	
R_p	22.0	R_p (profile factor)$=100[\Sigma\lvert y_i-y_{ic}\rvert/\Sigma\lvert y_i\rvert]$, where y_i is the observed intensity, and y_{ic} is the calculated intensity at the ith step.
R_{wp}	29.1	R_{wp} (weighted profile factor)$=100[\Sigma\omega_i\lvert y_i-y_{ic}\rvert^2/\Sigma\omega_i(y_i)^2]^{1/2}$, where $\omega_i=1/\sigma_i^2$ and σ_i^2 are the variance of observation.
R_{exp}	18.8	R_{exp} (expected weighted profile factor)$=100[(n-p)/\Sigma\omega_i(y_i)^2]^{1/2}$, where n and p are the number of profile points and refined parameters, respectively.
R_B	0.140	R_B (Bragg factor)$=100[\Sigma\lvert I_{obs}-I_{calc}\rvert/\Sigma\lvert I_{obs}\rvert]$, where I_{obs} is the observed integrated intensity, and I_{calc} is the calculated integrated intensity.
R_F	0.130	R_F (crystallographic R_F factor)$=100[\Sigma\lvert F_{obs}-F_{calc}\rvert/\Sigma\lvert F_{obs}\rvert]$, where F is the structure factor, $F=\sqrt{(I/L)}$, where L is Lorentz polarization factor.
χ^2	2.28	$\chi^2=\Sigma\omega_i(y_i-y_{ic})^2$.
d	1.9555	d (Durbin–Watson statistics)$=\Sigma\{[\omega_i(y_i-y_{ic})-\omega_{i-1}(y_{i-1}-y_{ic-1})]^2\}/\Sigma[\omega_i(y_i-y_{ic})]^2$.
Q_D	1.8824	Q_D=expected d.
S	1.5479	S (goodness of fit)$=(R_{wp}/R_{exp})$.